electronics

MDPI

Article

An Unobtrusive, Wireless and Wearable Single-Site Blood Pressure Monitor Based on an Armband Using Electrocardiography (ECG) and Reflectance Photoplethysmography (PPG) Signal Processing

Angelito A. Silverio [1,2,*], Consuelo G. Suarez [3], Lean Angelo A. Silverio [4], Joseph Y. Dino [2], Justine B. Duran [2] and Giuseppe Edgardo G. Catambing [2]

[1] Department of Electronics Engineering, Faculty of Engineering, University of Santo Tomas, Manila 1008, Philippines
[2] Research Center for the Natural and Applied Sciences, University of Santo Tomas, Manila 1008, Philippines
[3] Faculty of Medicine and Surgery, University of Santo Tomas, Manila 1008, Philippines
[4] Department of Neurological Surgery, Davao Doctors Hospital, Davao City 8000, Philippines
* Correspondence: aasilverio@ust.edu.ph

Abstract: Wearable medical devices (WMDs) for healthcare applications have become ubiquitous, allowing remote, at-home, and real-time chronic monitoring that have significantly decongested clinics. These WMDs permitted the monitoring of several physiological parameters, such as heart and respiration rates, SPO_2, temperature, and energy expenditure during activities of daily living (ADLs) or fitness activities. While the measurement of these parameters has become common, full noninvasive, unobtrusive, and real-time blood pressure (BP) monitoring remains elusive owing to BP's complex dynamics. To bring this into fruition, several works have been conducted combining different biosignals to indirectly extract BP by using PTT. Unlike previous works, we considered PTT variability by averaging it over discrete durations to account for BP variability for a more accurate estimation. PTTs were obtained using electrocardiograph (ECG) and reflective photoplethysmograph (rPPG) signals extracted by a wearable device attached to a single site on the upper arm. Our results show a significant correlation between average PTT and the BP measured using auscultation in a trial study. The developed system has potential for chronic, noninvasive, and cuff-less blood pressure monitors (BPMs) for localized and single-site implementations. Meanwhile, real-time data from the wearable device may be accessed via a remote desktop or a mobile phone application.

Keywords: wearable devices for healthcare; physiological signs monitor; electrocardiography; photoplethysmography; pulse transit time; blood pressure monitoring

Citation: Silverio, A.A.; Suarez, C.G.; Silverio, L.A.A.; Dino, J.Y.; Duran, J.B.; Catambing, G.E.G. An Unobtrusive, Wireless and Wearable Single-Site Blood Pressure Monitor Based on an Armband Using Electrocardiography (ECG) and Reflectance Photoplethysmography (PPG) Signal Processing. *Electronics* **2023**, *12*, 1538. https://doi.org/10.3390/electronics12071538

Academic Editor: J.-C. Chiao

Received: 28 November 2022
Revised: 16 December 2022
Accepted: 22 December 2022
Published: 24 March 2023

1. Introduction

1.1. Wearable Medical Devices

For the past decade, there has been a big boost in the wearable market for healthcare technologies. The global wearable medical device (WMD) market size was valued at USD 21.3 billion in 2021 and is expected to expand at a compound annual growth rate (CAGR) of 28.1% from 2022 to 2030 [1]. Meanwhile, the market size of cardiac WMDs exceeded USD 1.5 billion in 2020 and is anticipated to grow at a CAGR of over 24.7% between 2021 and 2027 [2]. Commercially available WMDs include fitness trackers, smart health watches, smart wearable systems incorporating sweat-based biosensors, etc. Such devices permit the real-time monitoring of several physiological biomarkers, including heart rate, temperature, SpO_2, respiration rate, step count, amount of energy expended, sweat analytes, etc.

Although it seems that such WMDs have become commonplace in personalized healthcare and fitness applications, issues such as accuracy and reliability remain avenues for research and development initiatives. A systematic review conducted by Fuller and

colleagues (2020) [3], showed that commercial wearable devices are accurate for measuring steps and heart rate in laboratory-based settings but vary depending on the manufacturer and device type. Meanwhile, in the strictest context of health and clinical decision making, it remains unusual to use the information from such WMDs. Furthermore, there is a need for the continued evaluation of the efficacy of WMDs to accurately and reliably measure purported outcomes [3].

To understand the accuracy and reliability issues that come with WMDs, one should be considering the various noise and interferences that are coupled at the interface of the tissue and the sensing electronics. These interface nonidealities constitute sensor offset and drift, lead migration, signal attenuation due to weak coupling, electromagnetic interference, power supply hum, and motion artifacts. Meanwhile, the level of signal attenuation is affected by the location of the sensor or the respective transduction media (e.g., light and vibration). Several sites tend to result in various signal-noise ratios for various biomedical signals.

1.2. Physiological Biomarkers

For the assessment of the health condition of an individual, diagnostic information is taken from these so-called physiological biomarkers, which come in a variety of forms, namely biopotential, biomechanical, and biochemical. The main bioelectrical signals are generated by the heart, the brain, and the muscles, producing electrocardiographs (ECGs), electroencephalographs (EEGs), and electromyographs (EMGs), respectively. These signals are characterized by low amplitudes typically in the microvolts (μV) to millivolts (mV) range and low bandwidths, from Hz to a few kHz ranges, as shown in Figure 1 [4]. Biomechanical signals originate from the mechanical function of the biological system. Examples of such signals include cardiac dynamics affecting blood pressure and cardiac output, which may be recorded via sonography and ballistocardiography (seismocardiography), and gait, which may be assessed by using data obtained from inertial measurement units (IMUs) or movement cameras. Finally, biochemical signals constitute variations in chemical concentrations of physiological analytes undergoing internal or external reactions, such as levels of glucose, sodium, potassium, etc.

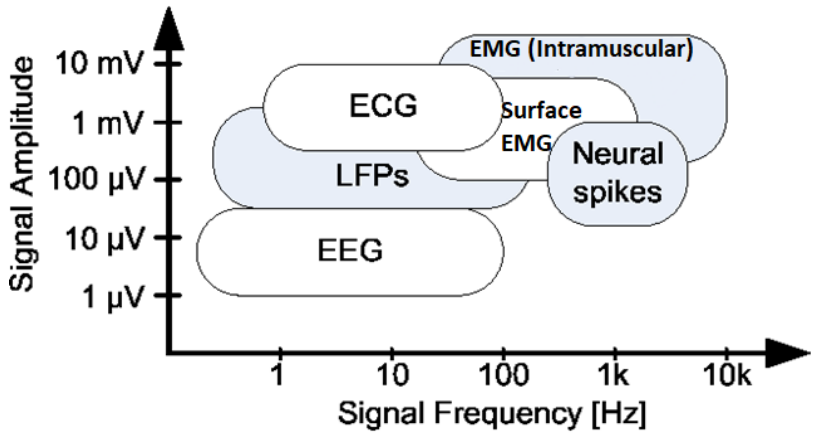

Figure 1. Biopotential signals signal level and bandwidth.

Electrocardiography signals have been thoroughly used in the assessment of heart conditions looking into the spatial characteristics of the PQRST waves from where heart rate (HR) and HR variability (HRV) are extracted. ECG signal acquisition has evolved from the conventional clinical device incorporating a desk-type or portable (e.g., Holter and handhelds) instrument with over 6 to 12 leads that are strategically positioned over the chest and wrists into the WMDs that come in the form of watches, arm bands, head gears, ear phones, etc., which are now part of everyday living. These WMDs can provide information on HR and HRV oftentimes used for fitness-tracking purposes. Research studies have even

sprung up exhibiting so-called smart textiles that permit chronic ECG monitoring, where the electrodes and sensing electronics are embedded in the clothing. Developments of these textiles are summarized in the review paper of Nigusse et al. (2021) [5]. Meanwhile, ECG electrodes on polyethylene glycol terephthalate (PET) surfaces may also be customized using a facile technique of developing metal patterns [6] or using graphene on flexible substrates [7].

While HR is measured clinically from the R-R interval of an ECG signal, concurrent technologies involving blood-flow variations (plethysmography) using light transmission or reflection, termed "photoplethysmography", or simply PPG, have offered a less intrusive approach. PPG systems use incident light having red, IR, or green wavelengths whose photons interact with the targeted tissue, causing either transmission, absorption, or reflection.

Commercially available WMDs use reflectance-mode PPG. Here, the intensity of reflected light is modulated by the blood-flow volume. The PPG signal comprises pulsatile (AC) and superimposed (DC) components. The AC component is provided by the cardiac synchronous variations in blood volume that arise from heartbeats. The DC component is shaped by respiration, sympathetic nervous system activity, and thermoregulation [8]. The AC component consists of systolic and diastolic peaks over a DC level. Various sites may be identified for obtaining good SNR for PPG measurements, as determined by the work of Longmore et al. (2019) [9]. Some of these potential sites for discernable rPPG signals are the wrist and shoulders. PPGs suffer from optical coupling and attenuation. Furthermore, ambient light cancelation is imperative for such systems to prevent them from saturating the photosensor.

Another biomedical signal for assessing heart function is based on the measurement of body motion generated by the ejection of the blood at each cardiac cycle, called ballistocardiography (BCG). It is one of the many methods relying on the detection of cardiac and cardiovascular-related mechanical motions, along with phonocardiography (recording of cardiovascular sound), apexcardiography (beat recording in the apex region of the heart through movements in the nearby wall of the chest), seismocardiography (recordings of the body vibrations induced by heart beats), and kinetocardiography (recordings of the absolute displacement of several points of the precordium) [10]. A common method to extract BCG signals is to use 3D accelerometers positioned on sites where pulsations may be felt. However, using such accelerometer sensors would require rigorous offset reduction, noise filtering, and motion-artifact reduction.

1.3. Methods of Extracting Pulse Transit Time (PTT)

The three biomedical signals (ECG, PPG, and BCG) may be used in tandem to extract the so-called pulse transit time (PTT), which directly correlates to the mean arterial pressure (MAP) [11]. PTT is the time delay for the arterial pressure wave (APW) to travel between two arterial sites and can be estimated simply from the relative timing between proximal and distal arterial waveforms [11]. The speed at which this APW travels was previously shown to have a strong relationship with BP. The work by Mukkamala and colleagues (2015) [11] have detailed the theory and practical implementation of PTT as a BP monitor. An acute rise in BP causes vascular tone to increase, and hence, the arterial wall becomes stiffer, causing the PTT to shorten. Conversely, when BP falls, vascular tone decreases and PTT increases [12]. A mathematical representation of the relation between BP and PTT is shown in Equation (1) [13]:

$$BP = -\frac{2}{\alpha}\ln PTT + \frac{\frac{\ln\left(2r\rho L^2\right)}{hE_0}}{\alpha} \quad (1)$$

where α is a constant, E_0 is the zero-pressure modulus of the vessel wall, L is the vessel length, ρ is the blood density, r is the inner radius of the vessel, and h is the vessel wall thickness. A simplified mathematical model for this relation is shown in Equation (2) [14]:

$$MAP = A - B \times \ln(PTT) + P_{hydro} \quad (2)$$

where MAP is the mean arterial pressure and A is a constant dependent on the elastic properties of the vasculature and the distance the pulse wave has traveled. B is also a constant dependent on elastic properties of the vasculature, and P_{hydro} is the hydrostatic pressure caused by gravity. These constants are experimentally obtained and are proportional to the elastic indices of the vasculature, which normally are 14.7 $\pm$ 5.2 ((mL/mm Hg) $\times$ 10) for large arteries and 4.9 $\pm$ 2.1 ((mL/mm Hg) $\times$ 100) for small arteries [15]. Meanwhile HR information may also be used to improve on the estimation of BP, as shown in Equation (3) [13]:

$$BPn = a \cdot \ln PTT + b \cdot HR + c \cdot BP_{n-1} + d \quad (3)$$

where BP_{n-1} is the previous BP estimate, and the four coefficients (a, b, c, and d) can be calculated by applying the least squares method.

Extracting BP through the PTT offers several advantages, such as unobtrusive monitoring because the inflatable cuff is unnecessary, noninvasiveness because no catheter is involved, and ubiquitous and continuous real-time BP monitoring. The challenge, however, is where to get enough signal with relatively high SNR and is least affected by motion artifacts. Furthermore, the PTT extraction mechanism should be attached to the area where signals are taken, to reduce the effect of interface nonidealities that causes such signals to drift, to be attenuated, and to be corrupted.

PTT may be extracted from a combination of ECG and PPG, measured as the time difference between the ECG's R-wave and the peak of the first running derivative of the PPG (see Figure 2a). Other methods utilize a pair of PPG signals located at two regions of the body, where the PTT is the time difference between the peaks of the corresponding signal derivatives [16], or the time interval between two pulse peaks of the PPG within the same cardiac cycle [17] (see Figure 2b). One work suggested the use of pulse intensity ratio (PIR) to account for the low-frequency (LF) variations in BP due to vasomotor tone, which is not accurately detected when using PTT systems [18]. Another method for PTT extraction is to use a combination of BCG and PPG, where the BCG sensor permits proximal arterial pulse waveform detection while the PPG is used to capture the distal pulse. PTT is the time difference between the proximal and distal pulse arrival times [19] (see Figure 2c). PTT may also be derived from using combination of ECG and BCG, where PTT is the time interval between the ECG's R-wave and the BCG's J-wave (see Figure 2c) [20]. Finally, the PTT may also be derived from the instance of the aortic opening through the BCG signal and the tangent of diastolic min from the PPG signal (see Figure 2d) [21].

1.4. Work Contribution

This work was able to demonstrate a viable wearable health monitor combining ECG and rPPG for the extraction of mean arterial pressure localized on a single arm. Blood pressure is extracted by using the pulse transit time (PTT) taken as the time difference between the appearance of the ECG R waves and the peak of the first derivative of the PPG signal. This work furthermore observed a correlation between the simultaneously measured blood pressure using standard cuff-based digital monitors and the various average PTTs over various constant duration time windows. By taking the average PTT (aPTT) over certain time windows, such measurements will have a higher correlation to BP because it takes into account the apparent variabilities of PTT, BP, and HR, which have nonlinear relationships. This work, however, was not able to correlate BP variability, because of limited access to clinical equipment. This work did not utilize commercially available WMDs that render real-time measurements of BP for its ground truth, as these are not the gold standards and are based mainly on mathematical estimations and approximations.

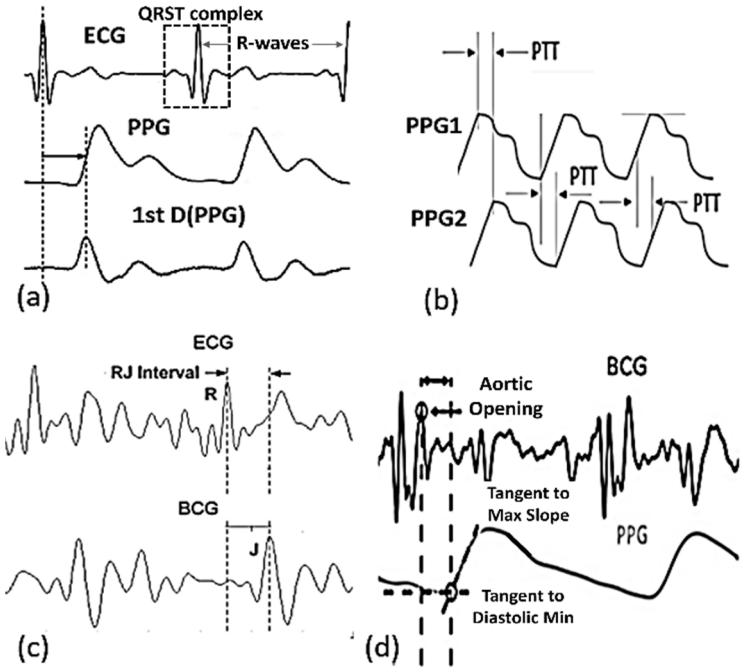

Figure 2. Methods for extracting PTT using combinations of biomedical signals: (**a**) using a combination of ECG and dPPG, (**b**) a combination of two PPGs, (**c**) a combination of ECG and BCG, and (**d**) a combination of BCG and PPG.

2. System Overview

2.1. Biomedical Signal Analog Front-End Design Considerations

Biomedical signals such as ECG and PPG have low amplitudes and frequencies. Typical ECG signals have an amplitude in the range of 0.5–4 mV with a bandwidth of 0.01–250 Hz; PPG signals have a pulse-wave frequency in the range of 0.5–4.0 Hz [22]. However, these frequency ranges are coincidental with the bandwidth of noise sources, namely flicker noise generated by circuit components (f_{corner} ~ 1 kHz), other interfering biopotential signals (e.g., sEMG), and motion artifacts (freq ~ 0.1 Hz). Hence, for such signals to be extracted, significant filtering and postprocessing must be performed. Meanwhile, PPG front ends must be able to attenuate ambient lighting as well as be very sensitive to weak changes in blood-flow volumes while rejecting other interfering signals. For PPG applications, normally red and IR are sufficient. However, for more-robust implementations, the green wavelength is used because it is the least affected by motion artifacts, when compared to red and IR.

2.2. Physiological Signs Monitoring System

For extracting the mean arterial pressure (MAP), a combination of electrocardioagram (ECG) and photoplethysmogram (PPG) signals has been used. The readout circuits are localized on a single site attached to the upper arm. For extracting the ECG, a three-electrode readout circuit was used on the basis of the AD8232 module. This is a low-power analog front end (AFE) with a typical current consumption of 170 uA at 2.5 to 3.0 V supply rail and high common-mode rejection (CMRR = 80 dB) suitable for in situ biopotential readout applications (e.g., wearable devices). The MAXREFDES117 dual-wavelength (red and IR) optical readout was used for extracting PPG (PPG) via reflection. It consists of the MAX30102 pulse oximeter and heart rate sensor that operates on 1.8 V supply rail with I^2C-compatible interface. Both readout circuits are driven by the Arduino Nano IOT 33 microcontroller unit (MCU) serving as a data logger and wireless interface. The MCU's main processor is a low-power Arm Cortex-M0 32-bit SAMD21 from Arm (Cambridge, UK). The Wi-Fi and Bluetooth connectivity is performed using the NINA-W10 module which is a low-power chipset operating in the 2.4 GHz range from u-blox (Thalwil,

Switzerland). On top of these, secure communication is ensured through the ATECC608B crypto chip from Microchip Technology Inc. (Arizona, USA). The MCU module also incorporates the LSM6DS3 3D inertial measurement unit (IMU) from STMicroelectronics (Geneva, Switzerland), which may be used for movement compensation or the extraction of BCG signals or for timing purposes. The fabricated system is shown in Figure 3 with the corresponding functional block diagram in Figure 4.

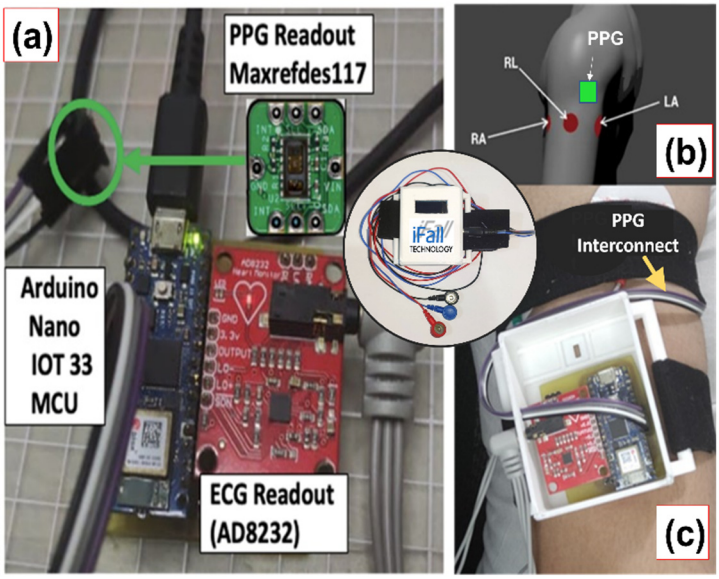

Figure 3. Fabricated device: (**a**) circuit overview, (**b**) electrode placement, (**c**) device placement onto the upper arm for data acquisition.

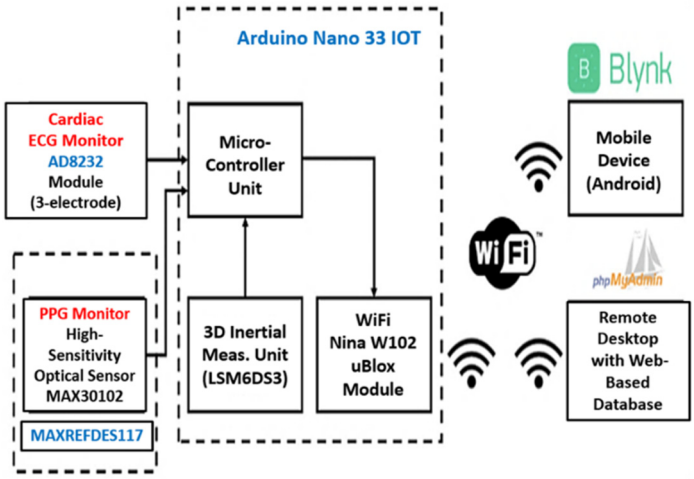

Figure 4. Wearable system block diagram showing the wireless interface via Wi-Fi to a mobile device and a desktop with a web-based database.

The fabricated device has a Wi-Fi interface connecting to both a remote desktop computer and a mobile phone. It can log in real time both the ECG data and the PPG data for use in postprocessing. A database has also been developed that can be used to log computed BP for various time periods.

2.3. PTT Extraction Methodology

The method for obtaining the PTT is summarized in Figure 5. It consists of the pre-scaling and denoising block for normalizing the extracted data and for the coarse removal of artifacts, a PPG fine-filtering block built on a 100th order FIR filter with cutoff frequencies

centered on the physiological PPG bandwidth (0.5 to 4 Hz), a block for extracting the running derivative of the PPG signal (dPPG), and blocks implementing the Pan–Tompkins algorithm (PTA) for the extraction of the respective time stamps of the ECG's R-wave and the dPPG peak, which are used to estimate the PTT. Data normalization is conducted by dividing the extracted ECG and dPPG signals by their corresponding maximum values for the entire duration. These signals may then be related or compared on the basis of their absolute values (from 0 to 1), thereby reducing any magnitude bias. The denoising block implements a prefiltering step to reduce artifacts. The PTT is taken as the time difference between the R-wave and the dPPG peak, as shown in Equation (4):

$$PTT_n = \frac{\left(T_{n(R-Wave)} - T_{n(dPPGpk)}\right)}{Fs} \quad (4)$$

where $T_{n(R-wave)}$ and $T_{n(dPPGpk)}$ are the respective time stamps of the detected R-wave and the peak dPPG, and F_s is the preset sampling frequency of the device (F_s = 200).

The Pan–Tompkins algorithm (PTA) is a peak detection algorithm. It recognizes specific complexes (comprising the significant peaks) of a signal on the basis of an analysis of the slope, amplitude, and width. PTA consists of a derivative filter followed by squaring function, moving window integration, and adaptive thresholds. The filtered biomedical signals are differentiated to obtain the signal components with high rates of change, which indicate the peaks. Then, the signals are squared to enhance these peaks. Moving window integration (MWI) is used to acquire information from the features of the waveform while removing other peaks that result from sensor sensitivity or ambient noise. The MWI width is crucial. We have chosen a width close to the typical duration of the QRS complex of the ECG signal and time duration between the systolic and diastolic peaks of the PPG signal. In lieu of these, the MWI width of 150 ms was used with the sampling rate of 200 samples/s.

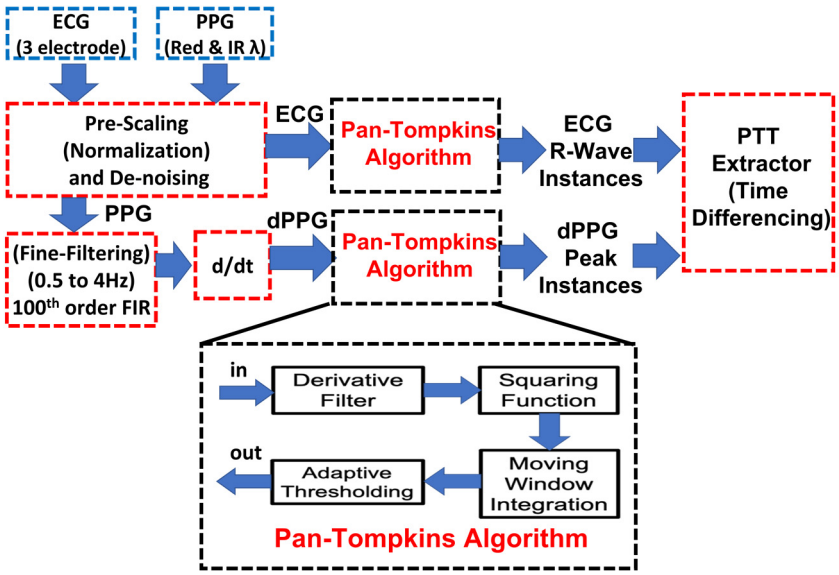

Figure 5. Pulse transit time (PTT) extraction methodology incorporating Pan–Tompkins algorithm for R-wave and dPPG peak detections.

3. Results and Discussion

Simultaneous ECG and PPG signals were experimentally obtained for 1 minute using two sets of configurations or test cases: three-electrode ECG collected on the chest area with the PPG collected on the wrist (test case 1 "TC-1") and where both ECG and PPG are collected on a single upper arm (test case 2 "TC-2"). For the single upper arm configuration, the ECG electrodes are positioned circumferentially with the PPG collected near the underarm (see Figure 2b). To obtain the conversion factor and linearity of the

extracted PTT with BP, the BP is obtained midway of the collection duration using standard cuff-based devices (Omron Smart Elite+ HEM-7600T Upper Arm Blood Pressure Monitor with Bluetooth Connectivity Digital BP).

The average PTT (aPTT) is obtained over a given duration and is correlated to SBP, MAP, and DBP. The MAP is calculated by using Equation (5) [23]:

$$\mathrm{MAP} = \frac{(\mathrm{SBP} + 2{*}\mathrm{DBP})}{3} \tag{5}$$

Only one subject was employed in this study. The subject had no reported physiological condition, such as hypertension, that would affect the measurements. The subject was within the age group of 20 to 30 years with a BMI of 30.9. The subject conducted the experiment in a stationary condition to avoid any potential signal artifact coming from micro- or macromotions. Both the aPTT and the natural log of aPTT (Ln(aPTT)) were compared with BP, as shown in Figures 6 and 7 for both test cases.

The extracted aPTTs of both test cases have significant correlations to the measured SBP, DBP, and MAP, as shown by their respective linear regression results. The absolute value of the Pearson correlation coefficient (r) is within 0.5 to 0.7, indicating a moderate correlation [24]. For both experimental setups, the aPTT correlated best with the MAP with correlation factors of r = 0.663 and r = −0.675 for TC-1 and TC-2, respectively. Similarly, the natural log of aPTT Ln(aPTT) correlated best with the MAP with correlation factors of r = 0.658 and r = −0.786, respectively. A higher r value was observed when correlating Ln(aPTT) with the BP. Usage of Ln(aPTT) is consistent with Equations (1) and (2), showing the linear relation between Ln(PTT) and BP.

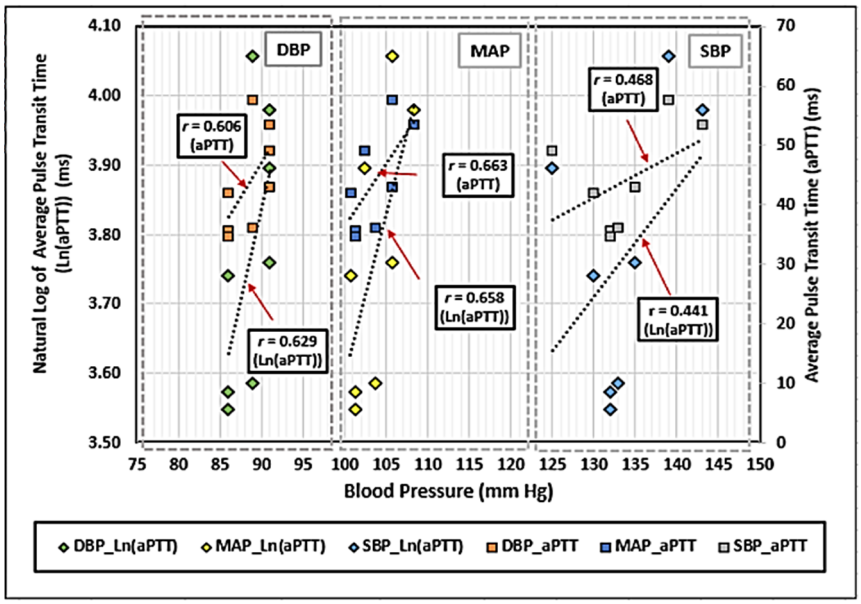

Figure 6. Plot of aPTT and Ln(aPTT) vs. BP where the ECG is extracted on the chest and the PPG on the wrist (test case 1 "TC-1") (n = 8 trials).

The correlation for TC-1 is positive but is negative for TC-2. This may be caused by the difference in displacement traveled by a PPG pulse wave as it traverses through either the arteries on the upper arm or those on the wrist. Negative *r*-values between PTT and BP have also been reported in the literature through the use of several sets of physiological modalities (e.g., ear and toe PTTs and dPPTs) [25]. Likewise, positive *r*-values have been reported in the literature when using a wrist PPG [26]. Another potential confounding factor to this is the inherent variabilities of BP [27], which tend to influence the PTT [28,29], as well as the effect of HR [11]. These PTT dependencies presuppose the need for gathering the average PTT over prescribed time windows to obtain better correlations with BP. This

was confirmed following the differences in correlations across various windows, as shown in Figures 8 and 9 for TC-1 and TC-2, respectively. Meanwhile the mean coefficient of variation (CoV) of the aPTTs per window further reveals PTT variability. The mean CoVs are 80% and 116% for TC-1 and TC-2, respectively. These CoVs mean that the aPTTs are significantly dispersed around the mean.

Following a one-factor analysis of variance (ANOVA), the *p*-values of these correlations per time window and BP across the entire data set were 0.029 (TC-1) and 0.847 (TC-2). These imply that for TC-1, there is a statistically significant difference in the *r*-values of the aPTT when correlated distinctively to SBP, DBP, and MAP, whereas for TC-2, there is no significant difference. The latter implies a possible 1:1 correspondence between the measured aPTT and either SBP, DBP, or MAP over a given time window.

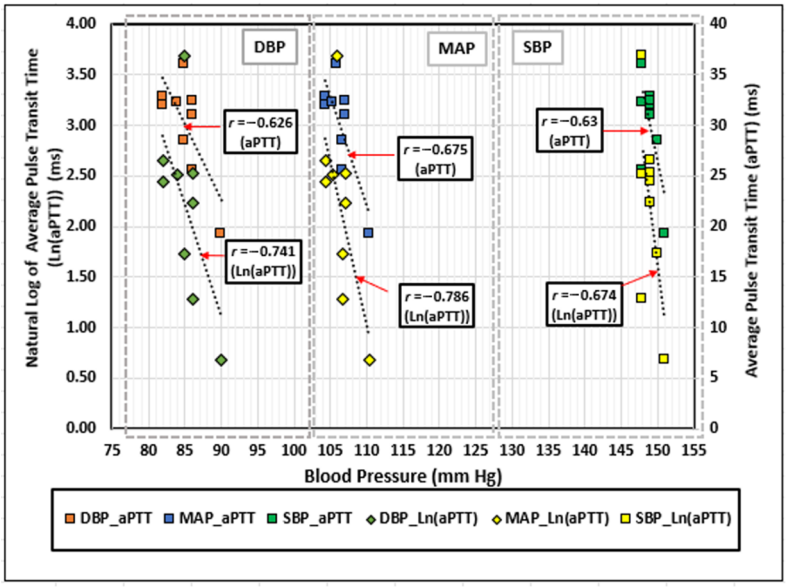

Figure 7. Plot of aPTT and Ln(aPTT) vs. BP where the ECG and PPG are both extracted on the upper arm (test case 2 "TC-2") (n = 9 trials).

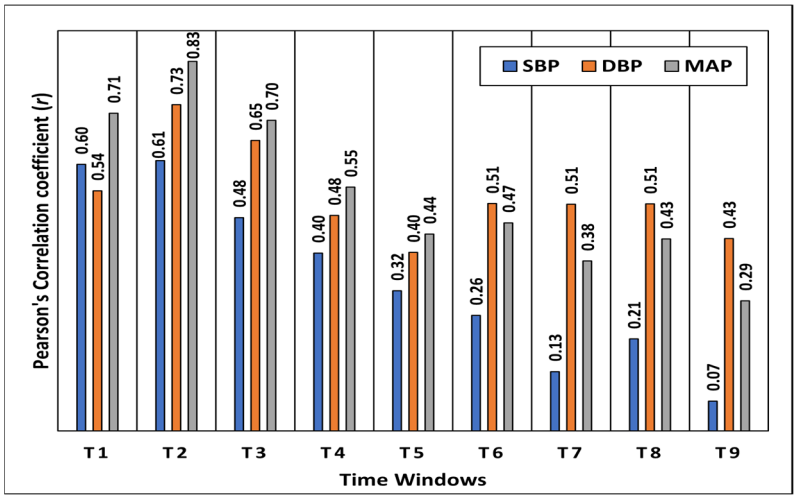

Figure 8. Correlations (*r*) of aPTT to BP at various time windows for TC-1.

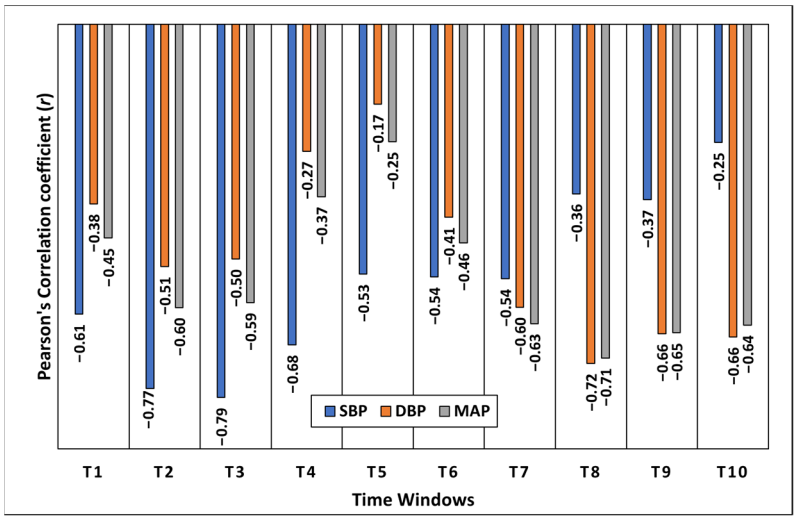

Figure 9. Correlations (*r*) of aPTT to BP at various time windows for TC-2.

4. Conclusions and Recommendations

This work demonstrated a viable unobtrusive and noninvasive method for estimating blood pressure using a combination of ECG and PPG extracted from the upper arm. This work was able to show the need for averaging the PTT over equal duration time windows to account for the inherent variability of BP, as shown by the significant differences in the resulting Pearson correlation factors between average PTT and average BP. This gives insight into when the average PTT must be taken alongside the averaging duration to provide better BP estimation. Most works, however, took the average PTT over the entire duration, which resulted in a low correlation owing to the apparent variabilities of PTT, BP, and HR and their nonlinear relationships. This work also showed the potential of using the Pan–Tompkins algorithm in determining the peaks of the dPPG for use alongside with the ECG's R-wave in the calculation of PTT. The results of this work conformed to those in the literature concerning the linear dependence of BP to PTT or Ln(PTT) extracted either from the single site (upper arm) or from proximal–distal sites.

To further improve the correlation between BP and PTT, it is suggested to include the effect of HR on both BP and PTT. Micro- and macromotion artifact cancelation algorithms may also be incorporated to achieve better correlations and higher SNRs.

Author Contributions: A.A.S. worked on the conceptualization, methodology, signal processing, formal analysis and journal paper writing; J.Y.D. worked on the methodology and data processing.; J.B.D. worked on the data collection and hardware development; G.E.G.C. worked on the initial system development and prototyping; L.A.A.S. provided guidance on the physiological aspects and the initial proofreading. C.G.S. assisted in the project conceptualization, development of protocols, and the final proofreading of the manuscript. All authors have read and agreed to the published version of the manuscript.

Funding: This research was funded by the Department of Science and Technology (DOST), Philippine Council for Health Research and Development (PCHRD), under the grant no. 21-0523.

Informed Consent Statement: Informed consent was obtained from all subjects involved in the study. Written informed consent has been obtained from the patient to publish this paper.

Data Availability Statement: Not applicable.

Acknowledgments: The authors acknowledge the Research Center for Health Studies, University of Santo Tomas, for the technical support, specifically during the project proposal phases and the protocol development. The authors also acknowledge the Philippine Council for Health Research and Development (PCHRD) of the Department of Science and Technology (DOST) for the project grant.

Conflicts of Interest: The authors declare no conflict of interest.

References

1. Grand View Research. Wearable Medical Device Market Size, Share & Trends Analysis Report by Type (Diagnostic, Therapeutic), by Site (Handheld, Headband, Strap, Shoe Sensors), by Application, by Region, and Segment Forecasts, 2022–2030. Available online: https://www.grandviewresearch.com/industry-analysis/wearable-medical-devices-market (accessed on 22 November 2022).
2. Global Market Insights. Wearable Cardiac Devices Market Size by Product (Holter Monitors, Patch, Defibrillators), by Application (Home Healthcare, Remote Patient Monitoring), COVID-19 Impact Analysis, Regional Outlook, Application Potential, Price Trends, Competitive Market Share & Forecast, 2021–2027. Available online: https://www.gminsights.com/industry-analysis/wearable-cardiac-devices-market (accessed on 22 November 2022).
3. Fuller, D.; Colwell, E.; Low, J.; Orychock, K.; Tobin, M.A.; Simango, B.; Buote, R.; Van Heerden, D.; Luan, H.; Cullen, K.; et al. Reliability and validity of commercially available wearable devices for measuring steps, energy expenditure, and heart rate: Systematic review. *JMIR mHealth uHealth* **2020**, *8*, e18694. [CrossRef] [PubMed]
4. Harrison, R. A versatile integrated circuit for the acquisition of biopotentials. In Proceedings of the 2007 IEEE Custom Integrated Circuits Conference, San Jose, CA, USA, 16–19 September 2007; pp. 115–122. [CrossRef]
5. Nigusse, A.B.; Mengistie, D.A.; Malengier, B.; Tseghai, G.B.; Langenhove, L.V. Wearable smart textiles for long-term electrocardiography monitoring—A review. *Sensors* **2021**, *21*, 4174. [CrossRef] [PubMed]
6. Sun, J.; Li, Y.; Liu, G.; Chen, S.; Zhang, Y.; Chen, C.; Chu, F.; Song, Y. Fabricating high-resolution metal pattern with inkjet printed water-soluble sacrificial layer. *ACS Appl. Mater. Interfaces* **2020**, *19*, 22108–22114. [CrossRef] [PubMed]
7. Cui, T.-R.; Li, D.; Huang, X.-R.; Yan, A.-Z.; Dong, Y.; Xu, J.-D.; Guo, Y.-Z.; Wang, Y.; Chen, Z.-K.; Shao, W.-C.; et al. Graphene-based flexible electrode for electrocardiogram signal monitoring. *Appl. Sci.* **2022**, *12*, 4526. [CrossRef]
8. Allen, J. Photoplethysmography and its application in clinical physiological measurement. *Physiol. Meas.* **2007**, *28*, R1–R39. [CrossRef] [PubMed]
9. Longmore, S.K.; Lui, G.Y.; Naik, G.; Breen, P.P.; Jalaludin, B.; Gargiulo, G.D. A comparison of reflective photoplethysmography for detection of heart rate, blood oxygen saturation, and respiration rate at various anatomical locations. *Sensors* **2019**, *19*, 1874. [CrossRef] [PubMed]
10. Giovangrandi, L.; Inan, O.T.; Wiard, R.M.; Etemadi, M.; Kovacs, G.T. Ballistocardiography—A method worth revisiting. In Annual International Conference of the IEEE Engineering in Medicine and Biology Society. IEEE Engineering in Medicine and Biology Society. In Proceedings of the Annual International Conference, Boston, MA, USA, 30 August–3 September 2011; pp. 4279–4282. [CrossRef]
11. Mukkamala, R.; Hahn, J.O.; Inan, O.T.; Mestha, L.K.; Kim, C.S.; Töreyin, H.; Kyal, S. Toward ubiquitous blood pressure monitoring via pulse transit time: Theory and practice. *IEEE Trans. Bio-Med. Eng.* **2015**, *62*, 1879–1901. [CrossRef]
12. Smith, R.P.; Argod, J.; Pépin, J.; Lévy, P.A. Pulse transit time: An appraisal of potential clinical applications. *Thorax* **1999**, *54*, 452–457. [CrossRef] [PubMed]
13. Wang, R.; Jia, W.; Mao, Z.H.; Sclabassi, R.J.; Sun, M. Cuff-free blood pressure estimation using pulse transit time, and heart rate. In Proceedings of the International Conference on Signal Processing, Bangalore, India, 20–23 December 2014; pp. 115–118. [CrossRef]
14. Winokur, E.S.; He, D.D.; Sodini, C.G. Wearable vital signs monitor at the ear for continuous heart rate and pulse transit time measurements. In Proceedings of the Annual International Conference of the IEEE Engineering in Medicine and Biology Society, San Diego, CA, USA, 28 August–1 September 2012; pp. 2724–2727. [CrossRef]
15. Pang, M.Y.; Yang, F.Z.; Jones, A.Y. Vascular elasticity and grip strength are associated with bone health of the hemiparetic radius in people with chronic stroke: Implications for rehabilitation. *Phys. Ther.* **2013**, *93*, 774–785. [CrossRef] [PubMed]
16. Wibmer, T.; Doering, K.; Kropf-Sanchen, C.; Rüdinger, S.; Blanta, I.; Stoiber, K.M.; Rottbauer, W.; Schumann, C. Pulse transit time based continuous cuffless blood pressure estimation: A new extension and a comprehensive evaluation. *Sci. Rep.* **2017**, *7*, 11554. [CrossRef]
17. Xijian, F.; Tardi, T. Robust contactless pulse transit time estimation based on signal quality metric. *Pattern Recognit. Lett.* **2020**, *137*, 12–16. [CrossRef]
18. Ding, X.R.; Zhang, Y.T.; Liu, J.; Dai, W.X.; Tsang, H.K. Continuous cuffless blood pressure estimation using pulse transit time and photoplethysmogram intensity ratio. *IEEE Trans. Bio-Med. Eng.* **2016**, *63*, 964–972. [CrossRef] [PubMed]
19. Töreyin, H.; Javaid, A.Q.; Ashouri, H.; Ode, O.; Inan, O.T. Towards ubiquitous blood pressure monitoring in an armband using pulse transit time. In Proceedings of the 2015 IEEE Biomedical Circuits and Systems Conference (BioCAS), Atlanta, GA, USA, 22–24 October 2015; pp. 1–4. [CrossRef]
20. He, D.D.; Winokur, E.S.; Sodini, C.G. A continuous, wearable, and wireless heart monitor using head ballistocardiogram (BCG) and head electrocardiogram (ECG). In Proceedings of the 2011 Annual International Conference of the IEEE Engineering in Medicine and Biology Society, Boston, MA, USA, 30 August–3 September 2011; pp. 4729–4732. [CrossRef]
21. Carek, A.M.; Conant, J.; Joshi, A.; Kang, H.; Inan, O.T. SeismoWatch: Wearable cuffless blood pressure monitoring using pulse transit time. *Proc. ACM Interact. Mob. Wearable Ubiquitous Technol.* **2017**, *1*, 1–16. [CrossRef] [PubMed]
22. Moraes, J.L.; Rocha, M.X.; Vasconcelos, G.G.; Vasconcelos Filho, J.E.; de Albuquerque, V.; Alexandria, A.R. Advances in Photopletysmography signal analysis for biomedical applications. *Sensors* **2018**, *18*, 1894. [CrossRef]

23. Papaioannou, T.; Protogerou, A.; Vavuranakis, M.; Tousoulis, D. Mean arterial pressure estimation by a non-traditional formula and fractional pulse pressure. *J. Am. Coll. Cardiol.* **2016**, *68*, 668–669. [CrossRef]
24. Hinkle, D.E.; Wiersma, W.; Jurs, S.G. *Applied Statistics for the Behavioral Sciences*, 5th ed.; Houghton Mifflin: Boston, CA, USA, 2003.
25. Block, R.C.; Yavarimanesh, M.; Natarajan, K.; Carek, A.; Mousavi, A.; Chandrasekhar, A.; Kim, C.-S.; Zhu, J.; Schifitto, G.; Mestha, L.K. Conventional pulse transit times as markers of blood pressure changes in humans. *Sci. Rep.* **2020**, *10*, 16373. [CrossRef]
26. Pandey, R.K.; Chao, P.C.P. External temperature sensor assisted a new low power photoplethysmography readout system for accurate measurement of the bio-signs. *Microsyst. Technol.* **2021**, *27*, 2315–2343. [CrossRef] [PubMed]
27. Parati, G.; Stergiou, G.S.; Dolan, E.; Bilo, G. Blood pressure variability: Clinical relevance and application. *J. Clin. Hypertens.* **2018**, *20*, 1133–1137. [CrossRef] [PubMed]
28. Murakami, K.; Yoshioka, M. Pulse transit time variability on a range of heart rates between resting and elevated states. In Proceedings of the 2015 IEEE International Conference on Systems, Man, and Cybernetics, Hong Kong, China, 9–12 October 2015; pp. 1579–1582. [CrossRef]
29. Ma, H.T.; Zhang, Y.T. Spectral analysis of pulse transit time variability and its coherence with other cardiovascular variabilities. In Proceedings of the 2006 IEEE Engineering in Medicine and Biology Society, New York, NY, USA, 30 August–3 September 2006; pp. 6442–6445. [CrossRef]